Cell Reports, Volume *8*

Supplemental Information

Cryoelectron Microscopic Structures of Eukaryotic Translation Termination Complexes Containing eRF1-eRF3 or eRF1-ABCE1

Anne Preis, Andre Heuer, Clara Barrio-Garcia, Andreas Hauser, Daniel E. Eyler, Otto Berninghausen, Rachel Green, Thomas Becker, and Roland Beckmann

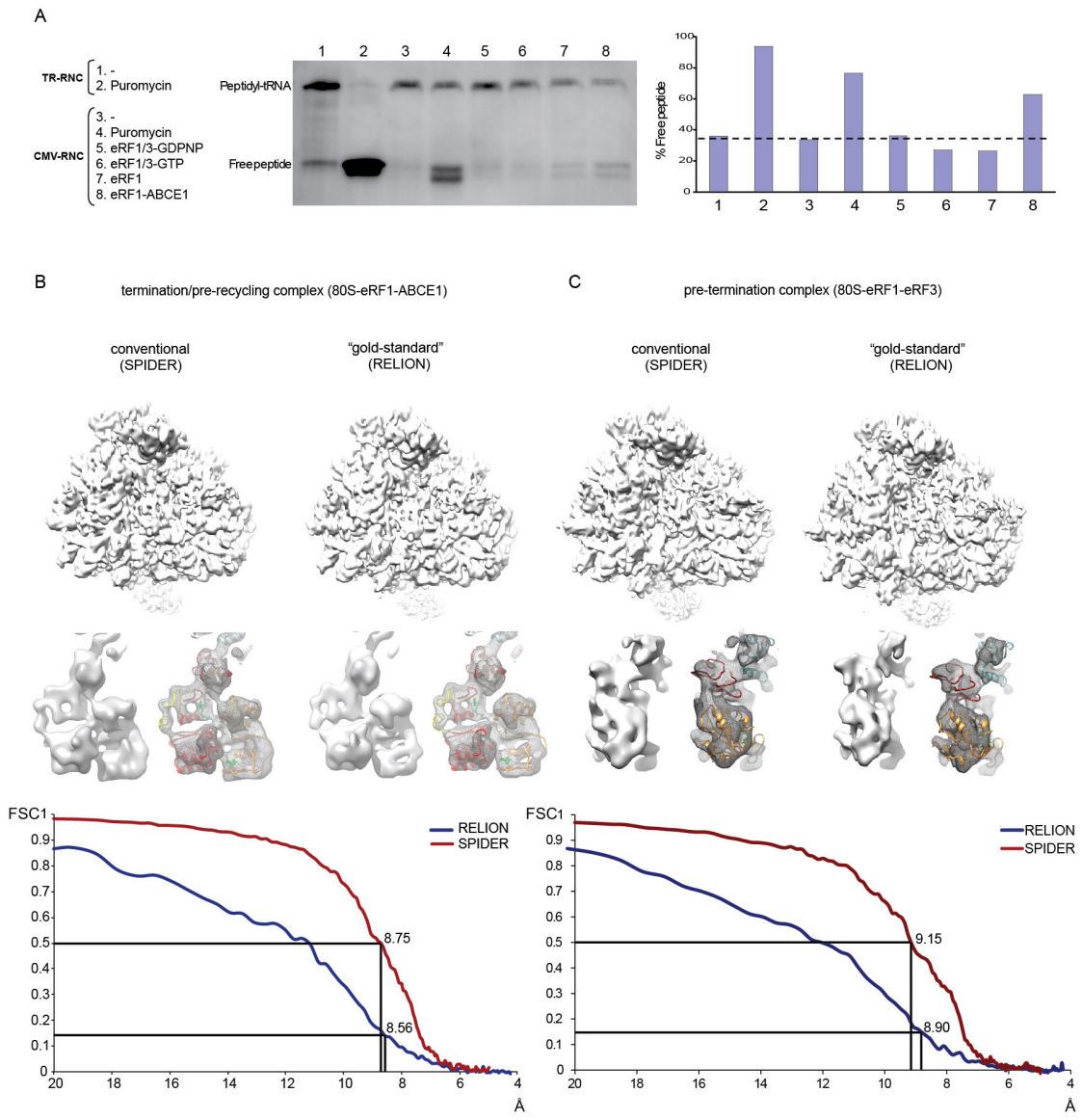

Figure S1 (related to Results and Discussion, Experimental Procedures and Figure 1) : Release Assays and Comparison between conventional refinement and "gold-standard" refinement (B,C)

"CMV-stalled" RNCs with a stop-codon in the A-site were either treated with puromycin or incubated with a 5-fold molar excess of release/recycling factor complexes and subjected to Western Blot analysis using an anti-HA antibody (**A**). Bands for peptidyl-tRNA and free peptide are indicated. As a measure for release activity the relative amount of free peptide was quantified using ImageJ. As a control, RNCs stalled by truncated mRNA (TR-RNC) were used.

Cryo-EM maps and resolution curves resulting from conventional SPIDER and "gold-standard" RELION refinement are shown for (**B**) the termination/pre-recycling dataset and (**C**) the pre-termination dataset. Snapshots were taken from the entire ribosome, the ribosomal exit site and isolated densities for the ligands (ABCE1 in (**B**), eRF3 in (**C**).

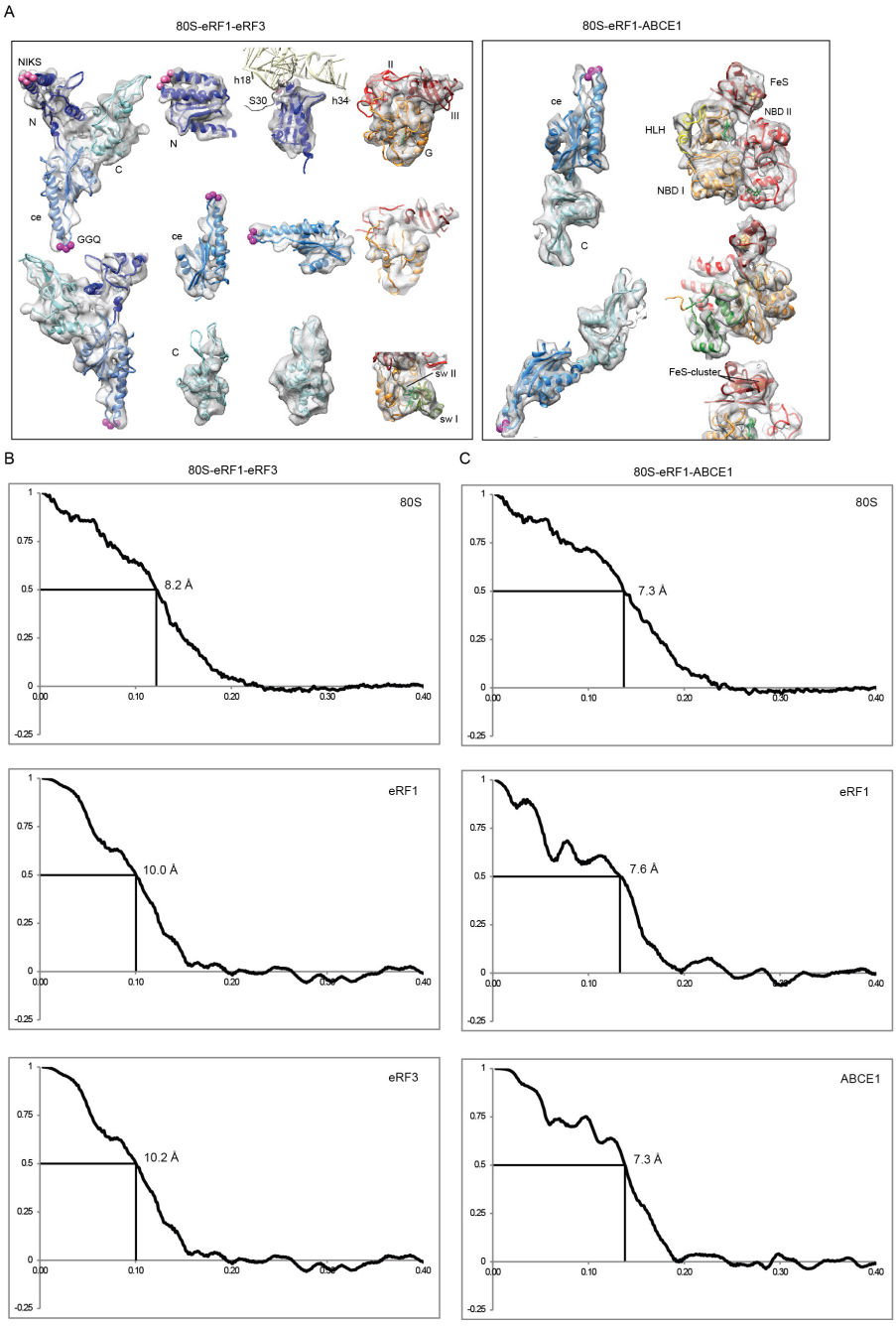

Figure S2 (related to Figures 1-3): Fitting of eRF1, eRF3 and ABCE1 and FSC curves between experimental maps and molecular models.

Isolated densities for eRF1, eRF3 and ABCE1 are shown in transperent mesh with homology models fitted based on resolved secondary structure. The color code for individual domains is as in **Figure 1B.** In addition, for the eRF1-NTD the ribosomal interaction site is shown. The mini-domain insert of the eRF1-CTD can only be seen with low contour levels. Density for the two FeS-clusters of ABCE1 is shown in red mesh. Nucleotides (GDPNP for eRF3, ATP for ABCE1) are shown in green.

FSC curves between models and maps for the 80S-eRF1-eRF3 dataset (**B**) and the 80S-eRF1-ABCE1 dataset (**C**) were calculated for the entire 80S ribosome using the model for the wheat germ ribosome (3J5Z, 3J60, 3J61 and 3J62) and for individual ligands. For ligands, respective densities were cut out using a soft mask and the resolution was read at a cutoff at a FSC 0.5.

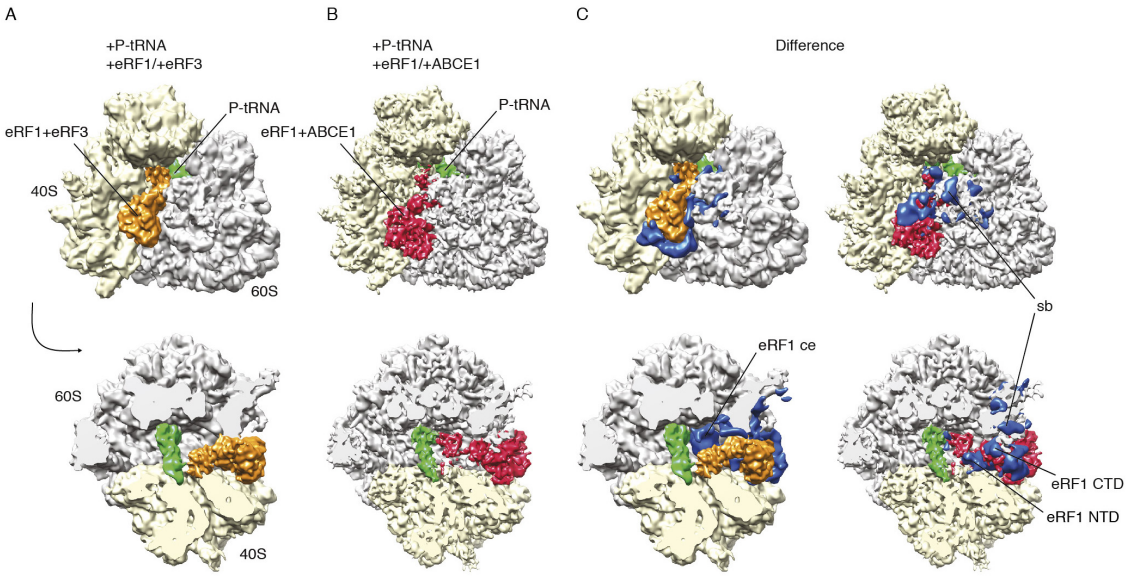

Figure S3 (related to Figure 1): Difference maps.

Front and top views of pre-termination (**A**) and termination/pre-recycling (**B**) complexes. In (**C**) the difference map of (**B**) minus (**A**) is shown in blue. Differences can be seen for the ribosomal stalk base (rRNA helices H43-H44 and r-protein L11), the eRF1 central domain and ABCE1. (**D**) represents the difference map (**A**) minus (**B**). Differences can be seen for the ribosomal stalk base (sb), eRF3 and the CTD and the NTD of eRF1.

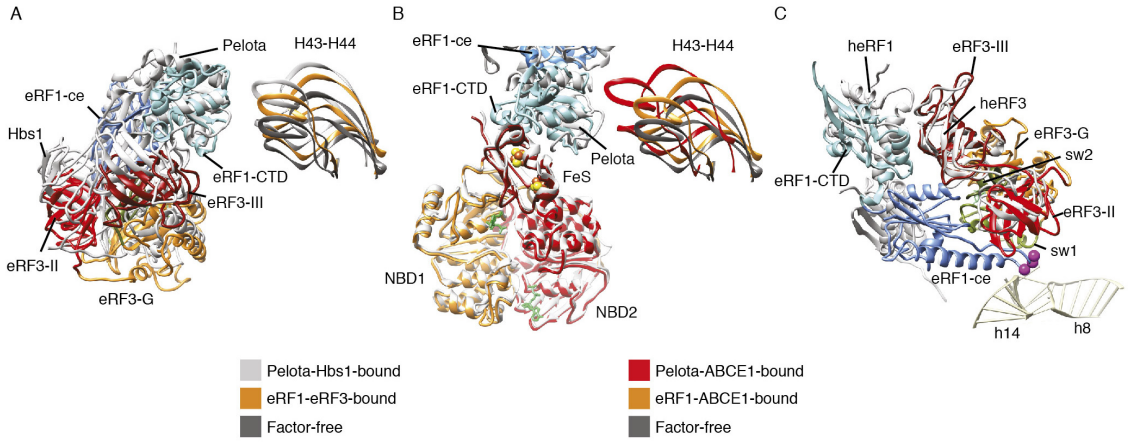

Figure S4 (related to Figures 2 and 3): Comparative analysis of ribosome-bound eRF1-eRF3 and eRF1-ABCE1 complexes.
(**A**) Overlay of the model for eRF1-eRF3 (color code as in **Figure 1B**) with Pelota-Hbs1 (PDB accession 3IZQ) (*17*) (grey). (**B**) Overlay of eRF1-ABCE1 (color code as in **Figure 1B**) with Pelota-ABCE1 (PDB accession 3J16) (*18*) (grey). The position of stalk-base helices H43-H44 in given in dark grey (factor-free), orange (bound to eRF1-eRF3), grey (bound to Pelota-Hbs1) and red (bound to eRF1-ABCE1 or Pelota-ABCE1). (**C**) Overlay of model for eRF1-eRF3 with the crystal structure of the human eRF1-eRF3 complex (PDB accession 3E1Y) (*12*) lacking the eRF3-G domain (grey).

Movie S1 (related to Figure 4): Eukaryotic translation termination.

Table S1: Contacts in the RNC-eRF1-eRF3:GDPNP pre-termination complex (related to Figure 2).

Table S2: Contacts in the RNC-eRF1-ABCE1:ADPNP termination/pre-recycling complex (related to Figure 3).

Supplemental Experimental Procedures

Purification of CMV-stalled ribosome nascent chain complexes

Wheat germ ribosomes were programmed with mRNA containing the first 98 amino acids of dipeptityl-pepdidase (DPAP-B98) carrying a type II signal anchor sequence followed by the 22-codon long human CMV *gp48* uORF stalling sequence. The template also encoded for N-terminal hexahistidine (His_6) and hemeagglutinin (HA) tags. The PCR-amplified DNA template was used for synthesis of uncapped mRNA using T7 RNA polymerase. RNCs were purified from the wheat germ cell-free translation extract as described before (Bhushan et al., 2010).

RNCs stalled by truncated mRNA coding for the first 120 amino acids of DPAP-B (DP120) were generated as described before (Becker et al., 2009).

Purification of eRF1, eRF3 and ABCE1

eRF1 and eRF3ΔN97 were cloned into pTYB2 (part of the IMPACT system by NEB) between the NdeI and SmaI sites and individually overexpressed in *E coli* BL21(DE3). Expression was carried out in Terrific Broth and induced with IPTG at 16 ºC for 15 h. Cells expressing release factors were washed with cold 1 % KCl, resuspended in lysis buffer eRF1 (20 mM HEPES pH 7.5, 500 mM NaCl, 1 mM EDTA) or lysis buffer eRF3 (20 mM HEPES pH 7.5, 500 mM NaCl, 0.1 mM GTP) and lysed using a French press.

The lysate was clarified at 20,000 g for 30 min (Beckmann Type 45 Ti) and loaded on Chitin Beads (NEB), 2 ml bed volume per 1 l of expression culture. The column was washed with 20 column volumes (CV) of corresponding lysis buffer and 20 CV of wash buffer (20 mM HEPES pH 7.5, 1 M NaCl, 1 mM EDTA). The column was flushed with 3 CV of elution buffer (20 mM HEPES pH 7.5, 500 mM KCl, 1 mM EDTA, 50 mM DTT) and incubated for 16 h at 4 ºC. The factors were eluted with 6 CV of elution buffer, concentrated and exchanged into gel filtration buffer (20mM HEPES pH 7.5, 200 mM KCl, 2 mM DTT, 1.5 mM $MgCl_2$, 10% Glycerol) in Microspin centrifugal filter units (threshold 10,000, Invitrogen) in 10-minute steps at 2500 g (5417/R, Eppendorf). Prior to gel filtration, the factors were incubated together in gel filtration buffer in the presence of 500 µM GDPNP or GTP on ice for 15 min. The complexes were purified on a Superdex 200 10/300 GL column and stored in gel filtration buffer. ABCE1 was purified from *S. cerevisiae* as described before (Shoemaker and Green, 2011).

Release assays

2 pmol RNCs were incubated with a ten-fold molar excess of eRF1-eRF3-GDPNP, eRF1 alone or eRF1 and ABCE1 in binding buffer (20 mM HEPES pH 7.5, 200 mM KCl, 1.5 $MgCl_2$, 2 mM DTT, 10 µg/ml cycloheximide, supplied with 500 µM GDPNP, GTP or ADPNP). Puromycin was added to a final concentration of 0.1 mM. The assays were incubated for 1 h at 27 ºC and analyzed by Western blot for HA-tag.

Reconstitution of RNC-eRF1-eRF3 and RNC-eRF1-ABCE1 complexes and cryo-EM sample preparation

RNCs were incubated with a ten-fold molar excess of preformed eRF1-eRF3 complex or eRF1 and ABCE1 in grid buffer (20 mM HEPES pH 7.5, 200 mM KCl, 1.5 $MgCl_2$, 2

mM DTT, 10 µg/ml cycloheximide, 0.05 % Nikkol, 0.03 % DBC, 500 µM GDPNP/ADPNP). Sec61 was added at a five-fold molar excess to saturate the hydrophobic signal-anchor sequence and avoid orientational bias on the cryo-grids.

Electron microscopy and image processing

For sample preparation, 2nm-carbon coated Quantifoil grids were used. The grids were prepared as described before (Wagenknecht et al., 1988). Both datasets were collected at 200 keV at a magnification of 147,136 × at the plane of the CCD using a TemCam-F416 CMOS camera (TVIPS GmbH, 4096 × 4096 pixel, 15.6 µm pixel, 1 s/full frame) resulting in an image pixel size of 1.06 Å (object scale). The particles were picked with starfish_boxing version 0.2.0, which is part of the new StarFish single particle analysis program suite. Starfish_boxing detects electron dense features by binarizing the raw micrographs into pixels with a value above an expected threshold and below. The binarization of the micrograph uses two arithmetic mean filtered images representing foreground and local background and are computed with either a very fast real space SSE2 implementation of with an FFT library. Only two parameters are required for a given dataset: the expected radius of the particle and a threshold for the binarization. After the binarization one usually gets many connected components ("white areas") in the shape of the densities present, e.g. particles, ice or similarly sized contamination. The connected components are then detected with a very simple algorithm. Based on the assumption that most connected components are particles a filter based on the median box size is used to filter out non-particles. The final coordinates were used for boxing out the particle images followed by import into SPIDER (Frank et al., 1996).

The RNC-eRF1-eRF3 dataset (224,689 particles) was sorted for presence of P-site tRNA first followed by sorting for the presence of factors. For the final reconstruction 39,309 particles were used. Sorting the RNC-eRF1-ABCE1 dataset (149,673 particles) was carried out analogously with 51,049 particles used for the final reconstruction.

The final datasets were also subjected to refinement using the "gold-standard" approach applied by the RELION software (Scheres, 2012). Here, the dataset is split into two data-subsets that are refined independently. The resolution was read at a FSC of 0.143 and, in good agreement with the results from conventional SPIDER processing, final resolutions after "gold-standard" processing were determined to 8.9 Å for the RNC-eRF1-eRF3 dataset and 8.6 Å for the RNC-eRF1-ABCE1 dataset.

Model building

For molecular interpretation of the *Triticum aestivum* 80S ribosome we used the updated model (pdb codes 3J5Z, 3J60, 3J61 and 3J62) (Gogala, 2014). Homology models of the central and NTD of eRF1 were built using HHPRED (Soding et al., 2005) on the basis of *Homo sapiens* and *Schizosaccaromyces pombe* crystal structures (Cheng et al., 2009; Song et al., 2000) (PDB accession 3E20 and 1DT9) The CTD (including the mini-domain insert that is not present in the crystal structures) was built on the basis of a NMR structure of the CTD of human eRF1 (PDB accession 2KTU) (Mantsyzov et al., 2010). The GGQ-loop (residues 177-183 of eRF1) was modeled based the GGQ-loop of RF2 (PDB accession 2XRT) (Jin et al., 2010) and RF1 (PDB accession 3MR8) (Korostelev et al., 2010). The eRF3 homology model was built on the basis of crystal structures of *S. pombe* Hbs1 (PDB accession 3MCA) (Chen et al., 2010) and eRF3 (PDB accession 1R5O) (Kong et al., 2004). Models for ABCE1 in the open ADP-bound, intermediate and closed ATP-bound state were described previously (Becker et al., 2012). Individual

domains of eRF1 and eRF3 were fitted as rigid bodies first and then manually adjusted using USCF Chimera (Pettersen et al., 2004) and Coot (Emsley and Cowtan, 2004). Final models were minimized in UCSF Chimera and clashes were removed using VMD (Phillips et al., 2005) and MDFF (Trabuco et al., 2008).

To validate the quality of the models the cross-resolution between the maps and the model was calculated. Using Chimera, we generated a map from the model-pdbs and calculated the resolution between these maps and our experimental maps. This was done for the entire ribosome as well as for individual factors eRF1, eRF3 and ABCE1. Isolated densities for the factors were extracted using soft masks in SPIDER.

SUPPLEMENTAL REFERENCES

Becker, T., Bhushan, S., Jarasch, A., Armache, J.P., Funes, S., Jossinet, F., Gumbart, J., Mielke, T., Berninghausen, O., Schulten, K.*, et al.* (2009). Structure of monomeric yeast and mammalian Sec61 complexes interacting with the translating ribosome. Science *326*, 1369-1373.

Chen, L., Muhlrad, D., Hauryliuk, V., Cheng, Z., Lim, M.K., Shyp, V., Parker, R., and Song, H. (2010). Structure of the Dom34-Hbs1 complex and implications for no-go decay. Nat. Struct. Mo.l Biol. *17*, 1233-1240.

Emsley, P., and Cowtan, K. (2004). Coot: model-building tools for molecular graphics. Acta. Crystallogr. D. Biol. Crystallogr. *60*, 2126-2132.

Gogala, M., Becker, T., Beatrix, B., Armache, J.-P., Barrio-Garcia, C.,Berninghausen, O. Beckmann, R. (2014). Cryo-EM structures of the Sec61-complex engaged in nascent peptide translocation or membrane insertion. Nature *506* 107-10.

Jin, H., Kelley, A.C., Loakes, D., and Ramakrishnan, V. (2010). Structure of the 70S ribosome bound to release factor 2 and a substrate analog provides insights into catalysis of peptide release. Proc. Natl. Acad. Sci. USA *107*, 8593-8598.

Korostelev, A., Zhu, J., Asahara, H., and Noller, H.F. (2010). Recognition of the amber UAG stop codon by release factor RF1. EMBO J. *29*, 2577-2585.

Pettersen, E.F., Goddard, T.D., Huang, C.C., Couch, G.S., Greenblatt, D.M., Meng, E.C., and Ferrin, T.E. (2004). UCSF Chimera--a visualization system for exploratory research and analysis. J. Comput. Chem. *25*, 1605-1612.

Phillips, J.C., Braun, R., Wang, W., Gumbart, J., Tajkhorshid, E., Villa, E., Chipot, C., Skeel, R.D., Kale, L., and Schulten, K. (2005). Scalable molecular dynamics with NAMD. J. Comput. Chem. *26*, 1781-1802.

Scheres, S.H. (2012). RELION: implementation of a Bayesian approach to cryo-EM structure determination. J. Struct. Biol. *180*, 519-530.

Trabuco, L.G., Villa, E., Mitra, K., Frank, J., and Schulten, K. (2008). Flexible fitting of atomic structures into electron microscopy maps using molecular dynamics. Structure *16*, 673-683.

Wagenknecht, T., Grassucci, R., and Frank, J. (1988). Electron microscopy and computer image averaging of ice-embedded large ribosomal subunits from Escherichia coli. J. Mol. Biol..*199*, 137-147.